Biosensors and Bioelectronics 142 (2019) 111491

Contents lists available at ScienceDirect

Biosensors and Bioelectronics

journal homepage: www.elsevier.com/locate/bios

A novel electrochemical sensor based on molecularly imprinted polymer modified hollow N, S-Mo_2C/C spheres for highly sensitive and selective carbendazim determination

Shuxiao Feng[a], Yangguang Li[c], Ruyue Zhang[d], Yingchun Li[b,*]

[a] College of Chemical Engineering & Pharmaceutical, Henan University of Science and Technology, Luoyang, 471023, China
[b] College of Science, Harbin Institute of Technology, Shenzhen, 518055, China
[c] Key Laboratory for Green Processing of Chemical Engineering of Xinjiang Bingtuan, School of Chemistry and Chemical Engineering, Shihezi University, Shihezi, China
[d] Key Laboratory of Xinjiang Phytomedicine Resource and Utilization, Ministry of Education, School of Pharmacy, Shihezi University, Shihezi, 832000, China

ARTICLE INFO

Keywords:
Molybdenum carbide
Carbon sphere
Nitrogen and sulfur doping
Molecular imprinting
Carbendazim detection
Pesticide residue

ABSTRACT

A novel electrochemical sensor based on nitrogen and sulfur doped hollow Mo_2C/C spheres (N, S–Mo_2C) and molecularly imprinted polymer (MIP) was proposed for carbendazim (CBD) determination. The N, S–Mo_2C were prepared by first nitrogen and sulfur doping via one-pot method and subsequent carbonization at high temperature. A film of MIP was then fabricated in situ on the N, S–Mo_2C surface by electropolymerization, with CBD acting as template molecule and *o*-phenylenediamine as functional monomer. The N, S–Mo_2C were characterized by scanning electron microscopy (SEM), transmission electron microscopy (TEM), energy-dispersive spectroscopy (EDS), X-ray diffraction (XRD), Fourier transform infrared spectroscopy (FT-IR), and electrochemical behaviors of CBD on differently modified electrodes were explored by cyclic voltammetry (CV) and electrochemical impedance spectroscopy (EIS). Under the optimal conditions, a calibration curve of current shift versus the logarithm of CBD concentration was obtained in the range of 1×10^{-12} ~ 8×10^{-9} M with a detection limit of 6.7×10^{-13} M (S/N = 3). Moreover, the proposed sensor exhibited favorable stability and selectivity, and was applied to analyze pesticide residues in fruits and vegetables with decent accuracy.

1. Introduction

Carbendazim (CBD) is a broad-spectrum benzimidazole fungicide and a metabolite of benomyl (Nemeth-Konda et al., 2002; Veneziano et al., 2004). It is widely used in agriculture for protecting from pathogens which would do harm to fruit and vegetables, and it can be absorbed by plants through roots, seeds and leaves, leading to long-term accumulation (Lim and Miller, 1997; Singh et al., 2007). Studies have found high doses of CBD cause infertility and destroy testicles of laboratory animals. The Europe Union and other countries have established the strict maximum residue limit of CBD since discovering its detrimental effects (Li et al., 2010). Various methods, including high-performance liquid chromatography (Bushway et al., 1991), spectrophotometry (Meszlényi et al., 1990), surface-enhanced Raman scattering (Strickland and Batt, 2009) and capillary electrophoresis (Oliveira et al., 2017), have been employed to monitor the content of CBD. However, they often suffer limitations including time consuming procedure, high-priced equipment and laborious pretreatment of bio-samples (Xu-Gang et al., 2008). In comparison, electrochemical analysis has unique features in respects of fast response, operational convenience, cost-effectiveness, low consumption of organic solvents, and easy miniaturization (Luo et al., 2013; Yao et al., 2014). However, selectivity is a common bottleneck issue accompanying sensor-based detection due to the fact that separation system is usually not involved in the analytical process (Yu et al., 2016).

Several articles reported the detection of CBD by electrocatalytic method which relies on its own electroactivity (Guo et al., 2011). However, high oxidation potential and low electroactivity hinder accurate and sensitive analysis of CBD, and poor selectivity results in the sensors not being able to identify target molecules out of the co-existing substances (Cui et al., 2017). Therefore, it is very important to modify electrochemical sensor with agents that can afford specific recognition toward analytes in complex environment (Zourob and Eissa, 2017). Various materials have been employed to play such function, including enzymes (Jie et al., 2018), antibodies (Özlem et al., 2016), nucleic acids (Zahid et al., 2016), molecularly imprinted polymers (MIPs) (Li et al.,

* Corresponding author.
E-mail address: liyingchun@hit.edu.cn (Y. Li).

https://doi.org/10.1016/j.bios.2019.111491
Received 3 April 2019; Received in revised form 9 June 2019; Accepted 1 July 2019
Available online 05 July 2019
0956-5663/

2016b), cyclodextrins (Zhang et al., 2018b), calixarenes (Zhang et al., 2016), etc. Among them, MIPs exhibit great potential due to its broad applicability to various substances, independence of analyte self-electroactivity, facile synthesis procedure, physical and chemical stability, and adaptability in harsh conditions (Hu et al., 2018; Li et al., 2018). In-situ electro-polymerization is a common way in preparing MIP-based electrochemical sensor, which is easy to operate and can be carried out at room temperature. The as-prepared MIP film has stable structure and is uniformly covered on electrode surface. Specifically, MIP-sensor synthesis includes first polymerization of functional monomers in the presence of template molecules and the subsequent removal of the template from MIP film, leaving behind imprinted cavities which are complementary in size, shape and functionality to the template. Sorption of template molecule onto the film inhibits transfer of probe ions (e.g. $Fe(CN)_6^{3-4-}$) to sensor surface, thereby impeding the redox reaction of probes and finally reducing their redox currents. Such so-called MIP-Gate effect system is a nice candidate tool for detecting CBD.

Additionally, high sensitivity and large detection capacity are other common requirements in sensor industry. In this respect, various modifiers, such as metal organic framework (MOF), metal oxides, carbon based nanomaterials, quantum dots, etc., have been used to decorate electrodes to improve sensing performances (Sharma et al., 2018). However, MOF and metal oxides need to be further carbonized or compounded with other materials due to poor conductivity (Indra et al., 2018; Qi-Long and Qiang, 2014), and quantum dots often suffer from poor stability (Bera et al., 2010; Li et al., 2015a). Among these modifiers, molybdenum-based nanomaterials, such as molybdenum disulfide (Lee et al., 2016), boride (Park et al., 2017), diselenide (Poorahong et al., 2017) and carbide (Mo_2C) (Li et al., 2016a), have become a hot spot in search of new inorganic catalytic materials thanks to their abundant reserves, admirable electrical conductivity and excellent catalytical ablility. Owing to low price, facile and efficient preparation, together with large surface, Mo_2C is one of the most widely used transition metal based materials in electrochemical region (Ma et al., 2016; Zhi et al., 2016). Some researchers have reported coupling Mo_2C with antigen for selectivity α-fetoprotein detection (Zhai et al., 2016), with Pt nanoparticles as durable catalyst for oxygen reduction reaction (Roy et al., 2013), and with graphitic carbon sheets as an efficient electrocatalyst for hydrogen generation (Wei et al., 2014). In order to pursue higher sensitivity, doping is an efficient way to control properties of nanomaterials (Huang et al., 2016; Samsudin et al., 2016), which expands the application of Mo_2C in electrochemical sensing. Moreover, studies have showed that hollow nanomaterials exhibited improved performance due to the increased surface area (Baca et al., 2018; Jiang et al., 2017). In this context, Mo-based hollow microspheres were synthesized, and the preparation included first nitrogen and sulfur doping and subsequent one-step pyrolysis, both of which improve catalytic and conductive properties of Mo_2C.

In summary, a newly electrochemical sensor was proposed by coupling MIP with nitrogen and sulfur doped hollow Mo_2C spheres (N, S–Mo_2C) for highly selective and sensitive determination of CBD. The easily fabricated MIP layer affords the sensor with ultra-specificity for CBD. And N, S–Mo_2C exhibit large surface area and great electrical conductivity, which elevates sensitivity and provides sufficient loading surface for MIP decoration. By taking advantages of the above mentioned two important elements, the manufactured sensor was successfully applied to assay CBD in vegetables and fruits. More significantly, it paves a great way to gauge species with low or no electroactivity, therefore extending the application potential of electrochemical sensor.

2. Experimental

2.1. Instruments and reagents

Carbendazim (CBD), thiophanate methyl (TPM), thiabendazole (TBZ), 2-aminobenzimidazole (2-ABZ), ethanol, $(NH_4)_6Mo_7O_{24}$ $4H_2O$ and dopamine were obtained from Alfa Aesar (Shanghai, China). All other chemicals used in this work, including $[Fe(CN)_6]^{3-/4-}$, thiourea, acetic acid, N, N-dimethyl formamide (DMF), KH_2PO_4, K_2HPO_4 and KCl, were bought from Adamas Reagent Co. Ltd. (Shanghai, China). Different grades of α-Al_2O_3 polishing powder were purchased from Sigma Aldrich Co. Ltd. (Titan, Shanghai). Commercially available CBD pesticides were bought at local pharmacies. Tomatoes, eggplants, cucumbers, grapes and apples were purchased from local supermarket. All the reagents were of analytical grade or better, and all solutions were prepared using double distilled water (DDW) and ultrasonicated by SY-360 Ultrasonic Cleaner (Shanghai Ningshang Ultrasonic Instrument Co., Ltd.). CBD was dissolved in acetic acid at a concentration of 1×10^{-3} M as stock solution, which was diluted to different concentrations with 0.1 M phosphate buffer before use.

Electrochemical measurements were carried out with a computer-controlled CHI 760E Electrochemical Workstation (CHI Instruments Co., Shanghai, China) at room temperature. A typical three-electrode cell was employed with a bare or modified glassy carbon electrode (GCE, 4 mm in diameter) as working electrode, a platinum wire as the counter electrode and a saturated calomel electrode (SCE) as reference electrode. Scanning electron microscopy (SEM, Zeiss Supra 55VP) and ransmission electron microscopy (TEM, JEM-1200EX) were applied for surface morphology characterization. Energy-dispersive spectroscopy (EDS, Scanning Electron Microscope, Zeiss Supra 55VP), Fourier transform infrared spectroscopy (FTIR, Nicolet iS10, Thermofisher, America) and X-ray diffraction (XRD, Rigaku Corporation, Tokyo, Japan) was used for element analysis. Brunauer-Emmett-Teller (BET) experiment was carried out at NOVA 1000 nitrogen adsorption specific surface area tester (Conta Instruments, USA) A centrifuge (Anke TGL-16G, China) was utilized to pretreat real samples.

2.2. Synthesis of N, S–Mo_2C

Preparation of N, S–Mo_2C included two steps. At first, the precursor, nitrogen and sulfur doped molybdenum-polydopamine hollow spheres (N, S-MPD), was synthesized and then carbonization in high temperature. Briefly, 0.25 g $(NH_4)_6Mo_7O_{24}$ $4H_2O$ was added in 40 mL DDW with ultrasonic treatment for 10 min, and the obtained solution was marked as solution A. 0.30 g dopamine and 0.30 g thiourea were dissolved in 20 mL DDW, and then the mixture was added dropwise to solution A with magnetically stirring at room temperature for 30 min to obtain a deep red solution. Subsequently, 150 mL of absolute ethanol was added to get a cloudy and orange solution. After stirring for 1 h, 0.4 mL of aqueous ammonia (25 wt%) was added to adjust the pH of the turbid solution to 8.5 ~ 9 and kept for 4 h. Then the product was collected by centrifugation at 8000 rpm and washed three times with ethanol and DDW in sequence, followed by drying in a vacuum furnace at 50 °C for 8 h. After that, the obtained N, S-MPD was placed in a tubular furnace at 900 °C under N_2 atmosphere with a heating rate of 5 °C min^{-1}, and the product was named as N, S–Mo_2C. For comparison, Mo_2C was prepared by the same method as that of N, S–Mo_2C except that thiourea was not added during precursor fabrication.

2.3. Fabrication of sensor

Bare GCE was sequentially polished to a mirror finish with 0.3 and 0.05 μm Al_2O_3, followed by ultrasonically washing with DDW for 3 min. And then 5 μL uniformly suspension of N, S–Mo_2C (1 mg mL^{-1}, dispersed in DMF) was dropped onto the surface of the treated GCE. After drying under infrared light for 5 min, the obtained N, S–Mo_2C modified GCE was marked as N, S–Mo_2C/GCE. MIP was synthesized via electropolymerization in phosphate buffer containing CBD (as template) and *o*-phenylenediamine (as functional monomer) by cyclic voltammetry (CV), which was carried out from 0 V to +0.8 V for 60 cycles at a scan rate of 50 mV s^{-1}. Subsequently, the electrode was placed in 1.0 M NaOH solution to remove template molecule CBD via CV scanning for

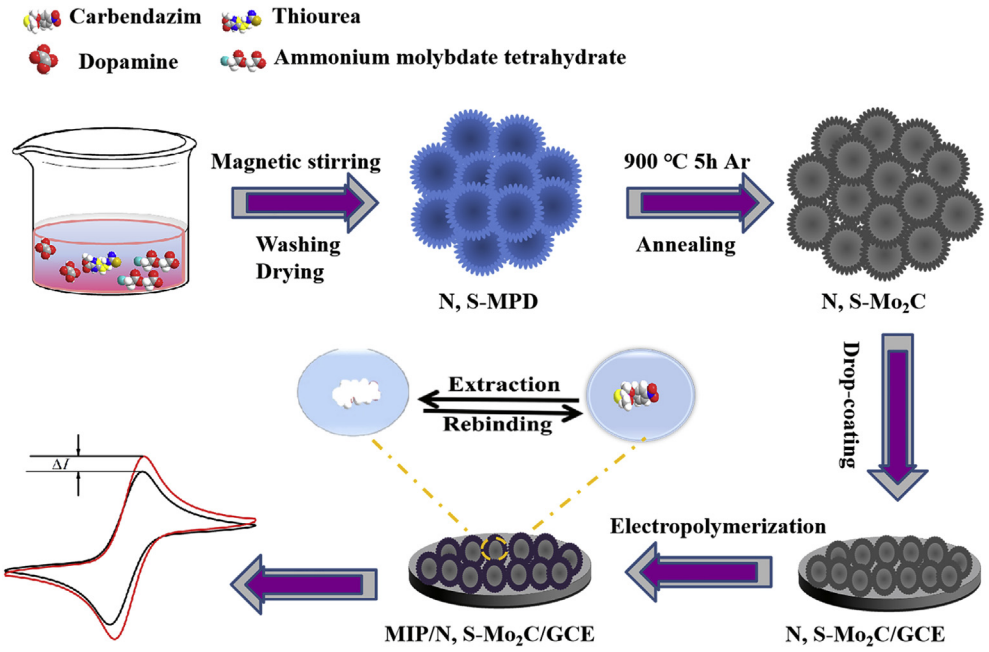

Fig. 1. Schematic preparation process of CBD-MIP/N, S–Mo_2C/GCE.

10 cycles in a potential range of −1.0 ~ +1.0 V until obvious and stable redox peaks were observed in the probe solution containing 5 mM $[Fe(CN)_6]^{3-/4-}$ and 0.1 M KCl. The schematic representation for preparing MIP modified sensor (MIP/N, S–Mo_2C/GCE) is shown in Fig. 1. Preparation of non-imprinted polymer (NIP) modified sensor (NIP/N, S–Mo_2C/GCE) was the same as that of MIP sensor except that CBD is not added during electropolymerization.

2.4. Electrochemical measurements

CV was applied to investigate electrochemical behavior of different electrodes in probe solution with scanning potential from −0.2 V to +0.6 V at scan rate of 100 mV s^{-1}. The peak current changes produced by $[Fe(CN)_6]^{3-/4-}$ ionic pair were used to evaluate binding ability of the modified sensor towards CBD or other structural analogues. Briefly, MIP/N, S–Mo_2C/GCE was first placed in CBD solution and incubated for 6 min, after which the electrode was rinsed with DDW to remove the surface-adhered residual material, and its current response in probe solution was recorded. The difference (ΔI) of the reduction peak current before and after incubation in CBD solution was used to explore sensor performances. After each analysis, the sensor was immersed in 1.0 M NaOH solution to removed CBD by CV in the range of −0.5 ~ +0.5 V for several cycles (about 6 cycles) until a stable redox peak can be observed in probe solution. The recovered sensor is then ready for the next assay. Electrochemical impedance spectroscopy (EIS) was also performed in probe solution within the frequence range from 0.01 Hz to 100 KHz. All the experiments were repeated for three times at room temperature.

2.5. Determination of CBD in real samples

In order to verify feasibility of the fabricated sensor in monitoring actual samples, the sensor was adopted to determine CBD in fruits and vegetables. The edible portion of samples was washed, dried in room temperature and juiced with a juicer. After that, 10 mL juice was mixed with 1 mL acetic acid and centrifuged at 8000 rpm for 15 min. The obtained supernatants were used for CBD analysis and stored at 4 °C when not in use. A certain amount of CBD was added to supernatants for the spiked recovery experiment.

3. Results and discussion

3.1. Characterization of CBD-MIP/N, S–Mo_2C/GCE

The preparation of N, S–Mo_2C included first nitrogen and sulfur doping by one-pot method and subsequent high-temperature pyrolysis. In Fig. S1A (Supplementary material file), MPD have an urchin-like structure with a diameter of about 600 nm. After carbonization, the morphology and structure of the obtained Mo_2C remains the same as that of MPD, while their diameter decreases to about 500 nm (Fig. S1B). Additionally, doping of nitrogen and sulfur has little impact on the morphology of the spheres (N, S-MPD in Fig. 2A and N, S–Mo_2C in Fig. 2B), and their shape is more similar to tennis ball with folding surface. Compared with N, S-MPD (with a diameter of about 400 nm), the morphology of N, S–Mo_2C has no obvious change after annealing, while the surface became rougher and their diameter decreases to around 350 nm. These changes could be the results of thermal decomposition of organic ligands, collapse of some organic skeletons and formation of small pores (Chao et al., 2016; Wang et al., 2017). TEM image in Fig. 2C confirms that N, S–Mo_2C manifests hollow core nanostructure with many lamellas. The elemental mapping in Fig. 2D exhibits uniform distribution of elements, including C, Mo, N and S. Their content was analyzed by EDS (Fig. S2A), which indicates that N and S were doped successfully. BET results of N, S–Mo_2C (Fig. S2B) and N, S-MPD (Fig. S2C) indicate an apparent increase in specific surface area after carbonization, with the area of 588.74 m^2g^{-1} and 254.31 m^2g^{-1}, respectively. The other changes accompanied with carbonization is enhancement of average pore size from 9 to 13 nm. FT-IR spectra for thiourea, MPD, Mo_2C, N, S-MPD and N, S–Mo_2C were recorded via KBr pellet method and shown in Fig. 2E. The above mentioned five species exhibit characteristic absorption peaks at 1615 cm^{-1} and 1445 cm^{-1} (İlktaç et al., 2017). This is due to the bending vibration of N–H and C–N, which proves the existence of indole structure after carbonization, and indicates successful introduction of N element. The characteristic absorption peaks of N, S-MPD and MPD at 1286 cm^{-1} are attributed to the bending vibration of O–H. After calcination at high temperature, the disappearance of absorption peaks at 1286 cm^{-1} of N, S–Mo_2C and Mo_2C indirectly indicates the partial thermal decomposition of organic ligands and the collapse of some organic skeletons. The adsorption band of N, S–Mo_2C and N, S-MPD at 1150 cm^{-1} suggests the

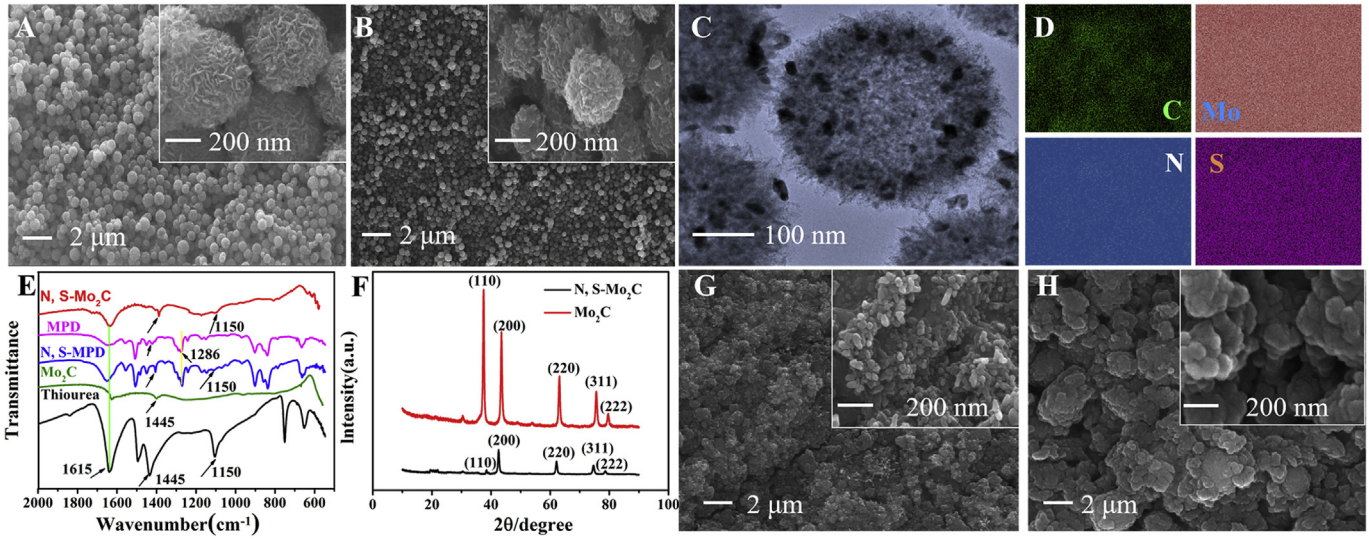

Fig. 2. SEM images of (A) N, S-MPD and (B) N, S–Mo_2C. (C) TEM images and (D) elemental mapping of N, S–Mo_2C. (E) FT-IR spectra of thiourea, MPD, Mo_2C, N, S-MPD and N, S–Mo_2C. (F) XRD spectra of Mo_2C and N, S–Mo_2C. SEM images of MIP-N, S–Mo_2C (G) before and (H) after extraction of CBD. The inset for each graph shows the image at higher resolution.

stretching vibration of C–S, which are consistent with characteristic absorption peaks of thiourea, indicating successful doping of S element. The XRD spectra of N, S–Mo_2C and Mo_2C were shown in Fig. 2F. The diffraction peaks at 37.76°, 43.69°, 63.39°, 75.72° and 79.86° correspond to (110), (200), (220), (311), (222) plane (Lin et al., 2016), which is in good agreement with JCPDS card (PDF#15-0457), and the result shows that N, S–Mo_2C were successfully synthesized. However, no obvious characteristic diffraction peaks of N and S were observed in XRD spectra of all the prepared samples, implying that introduction of N and S has little effect on the face-centered cubic structure of Mo_2C, which can be attributed to the low doping content.

The sensor was modified by utilizing a facile two-step coating procedure involving drop coating of N, S–Mo_2C and electropolymerization of MIP. As shown in Fig. 2G, after decoration of MIP, the surface of N, S–Mo_2C/GCE gets rougher with irregular shape, implying that MIP film was wrapped on the surface of N, S–Mo_2C/GCE. Subsequent extraction of CBD molecules resulted in more pores on the surface, and the increased surface porosity and pore size indicate that template molecules were successfully removed from the polymer (Fig. 2H).

To compare performances of the prepared materials, electrochemical behavior of electrodes modified with different materials was studied in probe solution via CV and EIS. Compared with bare GCE, the peak currents of the modified electrodes increased obviously (Fig. S3A), which is favorable to the enhancement of sensitivity (Wu et al., 2015). After doping of nitrogen and sulfur, responses obtained at N, S–Mo_2C/GCE and N, S-MPD/GCE were larger than Mo_2C/GCE and MPD/GCE, respectively, indicating that heteroatom doping plays an important role in raising electrical conductivity. After carbonization treatment, the peak currents at N, S–Mo_2C/GCE and N, S-MPD/GCE increased significantly compared with their respective precursor due to the enlarged surface area. Additionally, the largest current was obtained at N, S–Mo_2C/GCE owing to the synergistic effect of nitrogen and sulfur doping and one-step carbonization. Electron transfer properties were investigated via EIS (Liu et al., 2015), and the conclusion is consistent with that from the above CV results. The charge transfer resistance (R_{ct}) was estimated through calculating semicircle diameter. Randles equivalent circuit was used to fit all data obtained during EIS measurements (Inset of Fig. 3A) and the data were present in Table S1 with corresponding description. The sequence of R_{ct} values is bare GCE (R_{ct} = 97.81 Ω) > MPD/GCE (R_{ct} = 82.53 Ω) > N, S-MPD/GCE (R_{ct} = 77.16 Ω) > Mo_2C/GCE (R_{ct} = 45.23 Ω) > N, S–Mo_2C/GCE (R_{ct} = 38.58 Ω). As shown in Fig. 3A, the curve at N, S–Mo_2C/GCE showed almost a straight line, owing to boost in both conductivity and surface area of the electrode, which benefits sensing performance.

Electrochemical behaviors of the stepwised modification procedure of MIP sensor were explored in probe solution via CV. In Fig. S3B, the largest peak current was obtained at N, S–Mo_2C/GCE due to its large conductive surface area. After MIP modification, the redox peaks at MIP/N, S–Mo_2C/GCE significantly suppressed, implying that the polymeric film is non-conductive and covers almost the entire electrode surface. The subsequent extraction of CBD from MIP film destroyed the non-covalent interaction between polymer backbone and template, and the obtained imprinting cavities provided access for $[Fe(CN)_6]^{3-/4-}$, resulting in reappearance of peak current. When the MIP-decorated electrode was immersed in solution containing CBD, rebinding of CBD by MIP hindered the electron transport of probe ions, and thus the current value decreased.

To explore the role of nanoporous structure and the imprinting effect on sensor performances, the responses to CBD (6×10^{-12} M) at MIP/GCE, MIP/N, S–Mo_2C/GCE and NIP/N, S–Mo_2C/GCE were tested and compared (Fig. 3D). It is found that sensing responses (ΔI) obtained from the two MIP sensors were larger than that of NIP sensor, suggesting the existence of imprinted cavities and their adsorption ability toward CBD. In addition, we observed ΔI of MIP/N, S–Mo_2C/GCE ($\Delta I_{MIP/N,\ S-Mo2C/GCE}$ = 39.51 μA) is about twice larger than that of MIP/GCE ($\Delta I_{MIP/GCE}$ = 19.98 μA). This benefits from the enlarged electrode surface area due to N, S–Mo_2C modification.

3.2. Optimization of CBD-MIP/N, S–Mo_2C/GCE preparation

3.2.1. Optimization of pH value in electropolymerization for MIP preparation

In the electropolymerization process, the pH was first optimized under the conditions of a molar ratio of template to monomer (T: M) of 1 : 3 and a incubation time of 10 min (Zhang et al., 2018a). After polymerization and extraction of CBD, electrodes wrapped with different MIP films were utilized to analyze CBD (6.0×10^{-10} M). The ΔI of the reduction peak current before and after rebinding of CBD was calculated to estimate the effect of different pH in the range from pH 4.0 to pH 7.5. As shown in Fig. 4A, the largest response was obtained at pH 5.5, thus it was set for the following experiments.

3.2.2. Optimization of the ratio of T: M for MIP preparation

Ratio of template to monomer determines the amount of imprinted

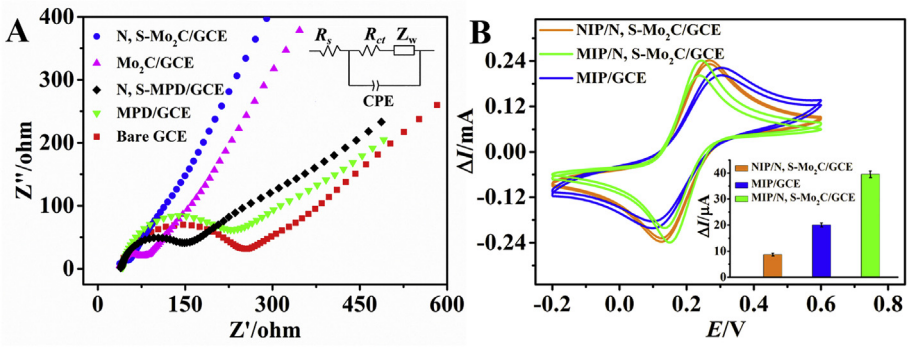

Fig. 3. (A) Nyquist diagrams of EIS of bare GCE, MPD/GCE, N, S-MPD/GCE, Mo_2C/GCE and N, S–Mo_2C/GCE. The inset is Randles equivalent circuit fitting with experimental data. (B) Cyclic voltammograms of MIP/GCE, MIP/N, S–Mo_2C/GCE and NIP/N, S–Mo_2C/GCE before and after binding of CBD. The inset is the corresponding sensing response of differently modified electrodes towards CBD. The supporting electrolyte of CV and EIS contained 5 mM $[Fe(CN)_6]^{3-/4-}$ and 0.1 M KCl. The scan rate of CV was 100 mV s^{-1} and the frequency range of EIS was from 0.01 to 100 kHz.

cavities in MIP layer, which affects the rebinding and recognition capabilities of MIP sensor. Insufficient amounts of functional monomer lead to insufficient number of binding sites that can be used to identify template molecules (Li et al., 2015b; Yujing et al., 2011). On the contrary, excessive monomers result in thick MIP films, and consequently many binding sites are buried in polymer matrix and become ineffective. Herein the ratio of T: M was optimized by testing the response of differently constructed sensor towards CBD (4.0×10^{-10} M). Fig. 4B implies that MIP/N, S–Mo_2C/GCE with *o*-phenylenediamine as a monomer brought out the highest response to CBD at T: M of 1 : 3 and the pH value of 5.5.

3.2.3. Optimization of incubation time

As shown in Fig. 4C, with the incubation time increased in the first 6 min, the response of MIP/N, S–Mo_2C/GCE to CBD (8.0×10^{-10} M) also increased, and the current remained essentially unchanged after 6 min, implying that at this time point the binding cavities in MIP have been completely occupied by template molecules, reaching saturation state (Li et al., 2018). Hence, 6-min incubation was adopted for analyzing CBD with the proposed MIP/N, S–Mo_2C/GCE.

3.3. Effect of scan rate

Effect of scan rate on MIP/N, S–Mo_2C/GCE was studied via CV in probe solution (Yang et al., 2017). It can be seen from Fig. 4D that both the anodic and cathodic peak currents increased linearly with the square root of scan rate varying from 10 to 150 mV s^{-1}. It indicates the binding reaction at the surface of MIP/N, S–Mo_2C/GCE to CBD is a diffusion controlled process.

3.4. Calibration curves and detection limit

Under the optimum experimental conditions, Different concentrations of CBD were determined by CV. Fig. 5A shows the linear correlation between ΔI and logarithm of the concentration of CBD (ln*C*), and the corresponding equation is ΔI (μA) = 5.2736 ln C + 153.84 (R^2 = 0.9959) in the range of 1×10^{-12} ~ 8×10^{-9} M. The limit of detection (LOD) was estimated to be 6.7×10^{-13} M based on signal-to-noise of 3 (S/N = 3). Moreover, the comparison of our method with other reported electrochemical sensors for CBD assay is summarized in Table S2. It is found that our sensor exhibits the lowest LOD and wider linear range compared with its counterparts.

3.5. Selectivity

Structural analogues of CBD, including TPM, TBZ and 2-ABZ, were selected as potential interferents to assay the selectivity of MIP/N, S–Mo_2C/GCE and NIP/N, S–Mo_2C/GCE. As illustrated in Fig. 5B, the MIP-modified sensor showed much higher response toward CBD (6×10^{-10} M) compared with other compounds, whereas the responses

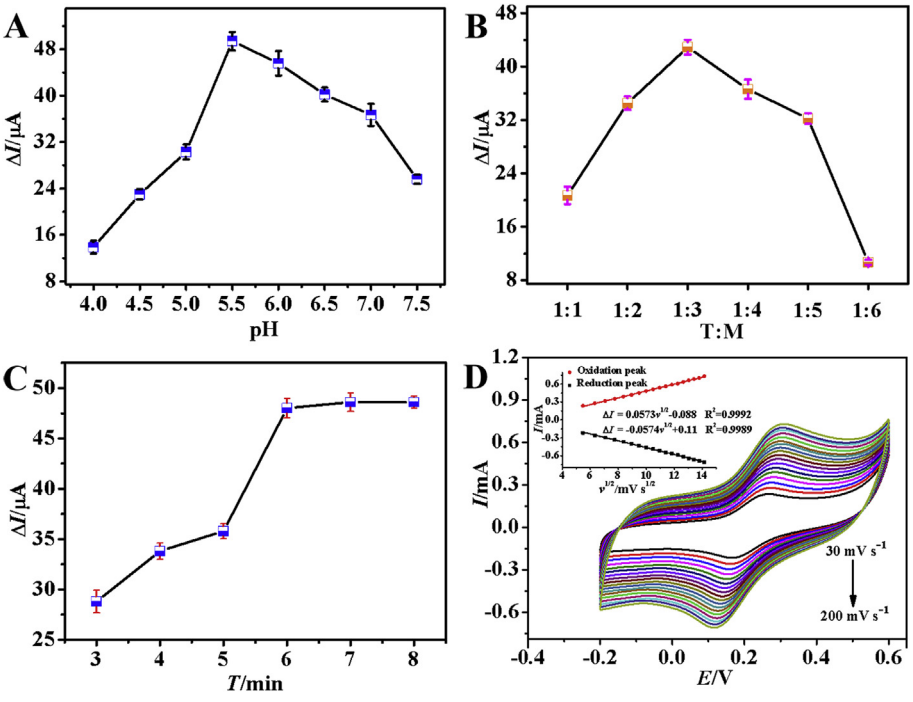

Fig. 4. Sensing responses toward CBD using different MIP/N, S–Mo_2C/GCE prepared (A) with varied pH values and (B) with varied ratios of T: M. The T: M was set at 1 : 3 for (B). (C) Optimization of incubation time during detection process. (D) Cyclic voltammograms of MIP/N, S–Mo_2C/GCE at different scan rates. The inset is the anodic and the cathodic peak currents versus square-root of scan rate plot. All the experiments were performed in triplicate.

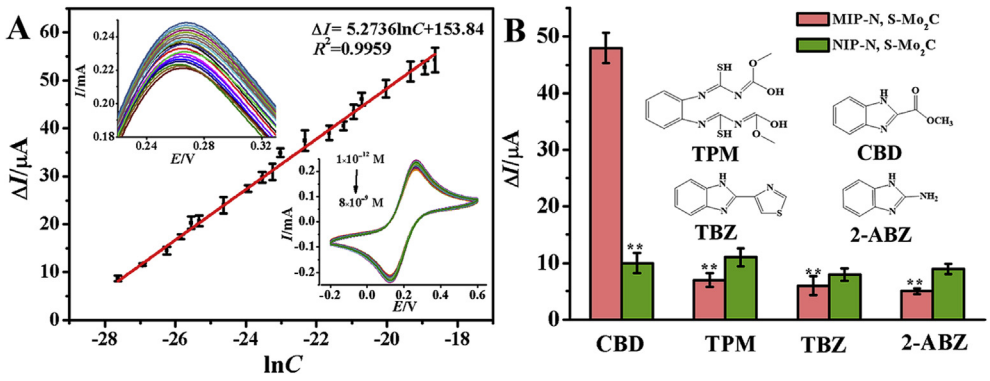

Fig. 5. (A) Calibration curves for CBD detection correlating ΔI with CBD concentration by using MIP/N, S–Mo_2C/GCE. The left inset shows partially amplified cyclic voltammograms and the right inset is the calibration curve correlating ΔI with ln$C$ of CBD. (B) Comparison of sensor responses towards CBD and its structural analogues at 6×10^{-10} M using MIP/N, S–Mo_2C/GCE and NIP/N, S–Mo_2C/GCE. The inset is chemical structures of CBD and its analogues.

of NIP-modified sensor hardly displayed any specificity among all the analytes. *T*-test of the results further confirmed that there was a significant difference in the sensing response between CBD and its analogues with a significant level of 0.01. High selectivity of the MIP-modified sensor stems from the recognition sites of MIP film, which matches the template molecule in space size and chemical function, but do not match other interferents.

3.6. Repeatability, reproducibility and stability

Repeatability was studied by measuring three different concentrations of CBD (4×10^{-9} M, 2×10^{-10} M and 6×10^{-12} M) for three times in succession, and the relative standard deviation (RSD) was less than 6.12%, indicating that the sensor affords excellent repeatability. To evaluate reproducibility, five different sensors were fabricated independently by the same process, and RSD of sensor responses to 2×10^{-10} M and 6×10^{-12} M CBD was 4.37% and 5.86%, respectively, which reveals the decent reproducibility of the sensor. Additionally, stability of the modified electrode was investigated by using the same sensor to detect 4×10^{-11} M CBD for 15 days continuously, and then it was stored at room temperature when not in use. After 15 days, response of the sensor is 94.3% of the initial response value with a RSD of 5.83%. This result indicates the robust stability of the modified electrode, which can be ascribed to the structural and compositional stability of N, S–Mo_2C and MIP layer.

3.7. Real sample analysis

To further explore the practical application, determination of CBD in fruits and vegetables was carried out via MIP/N, S–Mo_2C/GCE. The recoveries varying from 98.40 to 100.08% for grape, 95.45 to 97.74% for apple, 97.5 to 100.8% for tomatoes, 99.64 to 99.80% for eggplant and 95.20 to 98.19% for cucumber were showed in Table S4. The above results indicate that the designed MIP-modified sensor exhibits admirable accuracy and reliability for CBD detection in real samples.

4. Conclusion

In this work, a novel electrochemical sensor was proposed based on MIP and N, S–Mo_2C for highly selective and sensitive determination of CBD. To our knowledge, it is the first report on combination of Mo-based microspheres with MIP and adoption for pesticide residues analysis. Preparation of N, S–Mo_2C was simple including first nitrogen and sulfur doping and subsequent one-step pyrolysis and the process is highly controllable. The excellent electrochemical performance of N, S–Mo_2C can be attributed to its hollow and porous structure, which serves as high-surface-area matrix to help MIP layer decoration and accelerates electronic transmission. The generated polymeric layers provide many specific binding cavities, which complement the template CBD in space size and chemical function, thus ensuring good selectivity of the prepared sensors. Moreover, the as-prepared sensor was applied to analyze residual CBD in fruits and vegetables with satisfactory recoveries, which further proves the practicability and reliability of the sensor. Therefore, it can be expected that the developed sensor has great potential in a wide variety of fields including drug residue testing, food safety, therapeutic drug monitoring, drug quality control and environmental monitoring.

Declaration of interests

The authors declare that they have no known competing financial interests or personal relationships that could have appeared to influence the work reported in this paper.

CRediT authorship contribution statement

Shuxiao Feng: Conceptualization, Methodology, Software, Data curation, Writing - original draft, Writing - review & editing. **Yangguang Li:** Resources, Formal analysis. **Ruyue Zhang:** Data curation, Writing - review & editing. **Yingchun Li:** Project administration, Writing - review & editing, Supervision.

Acknowledgment

Financial supports from National Natural Science Foundation of China (81773680), Innovation and entrepreneurship project for overseas high-level talents of Shenzhen (KQJSCX20180328165437711) and Natural Science Foundation of Henan Province (No. 182300410353).

Appendix A. Supplementary data

Supplementary data to this article can be found online at https://doi.org/10.1016/j.bios.2019.111491.

References

Baca, M., Cendrowski, K., Kukulka, W., Bazarko, G., Moszyński, D., Michalkiewicz, B., Kalenczuk, R., Zielinska, B., 2018. Nanomaterials 8 (9), 639.
Bera, D., Lei, Q., Tseng, T.K., Holloway, P.H., 2010. Materials 3 (4), 2260–2345.
Bushway, R.J., Hurst, H.L., Kugabalasooriar, J., Perkins, L.B., 1991. J. Chromatogr. A 587 (2), 321–324.
Chao, J., Yong, L., Wang, Z.J., Yue, F., Qi, W., Yang, R., 2016. J. Mater. Chem. 4 (32), 12583–12590.
Cui, R., Xu, D., Xie, X., Yi, Y., Quan, Y., Zhou, M., Gong, J., Han, Z., Zhang, G., 2017. Food Chem. 221, 457–463.
Guo, Y., Guo, S., Li, J., Wang, E., Dong, S., 2011. Talanta 84 (1), 60–64.
Hu, X., Feng, Y., Wang, H., Zhao, F., Zeng, B., 2018. Anal. Methods-UK 10 (37), 4543–4548.
Huang, B., Xiao, L., Dong, H., Zhang, X., Wei, G., Mahboob, S., Al-Ghanim, K.A., Yuan, Q., Li, Y., 2016. Talanta 164, 601–607.
Indra, A., Song, T., Paik, U., 2018. Adv. Mater. 1705146.
İlktaç, R., Aksuner, N., Henden, E., 2017. Spectrochim. Acta 174, 86–93.
Jiang, Q., Li, L., Bi, J., Liang, S., Liu, M., 2017. Nanomaterials 7 (2), 24.
Jie, X., Gong, Q., Zhang, R., Shan, S., Zou, R., Wu, A., 2018. Chem. Commun. 54 (63), 8773–8776.

Lee, J.U., Kim, K., Han, S., Ryu, G.H., Lee, Z., Cheong, H., 2016. ACS Nano 10 (2), 1948–1953.
Li, H.F., Nie, J.Y., Xu, G.F., Li, J., 2010. Jiangsu J. Agr. Sci. 26 (2), 415–419.
Li, X., Rui, M., Song, J., Shen, Z., Zeng, H., 2015a. Adv. Funct. Mater. 25 (31), 4929–4947.
Li, Y., Liu, Y., Yang, Y., Yu, F., Liu, J., Song, H., Liu, J., Tang, H., Ye, B.C., Sun, Z., 2015b. Acs Appl. Mater. Inter. 7 (28), 15474–15480.
Li, J.S., Wang, Y., Liu, C.H., Li, S.L., Wang, Y.G., Dong, L.Z., Dai, Z.H., Li, Y.F., Lan, Y.Q., 2016a. Nat. Commun. 7, 11204.
Li, Y., Song, H., Zhang, L., Zuo, P., Ye, B.C., Yao, J., Chen, W., 2016b. Biosens. Bioelectron. 78, 308.
Li, Y., Liu, J., Zhang, Y., Gu, M., Wang, D., Dang, Y.Y., Ye, B.C., Li, Y., 2018. Biosens. Bioelectron. 106, 71–77.
Lim, J., Miller, M.G., 1997. Toxicol. Appl. Pharmacol. 142 (2), 401–410.
Lin, H., Shi, Z., He, S., Yu, X., Wang, S., Gao, Q., Tang, Y., 2016. Chem. Sci. 7, 3399–3405.
Liu, X., Qin, Y., Deng, C., Xiang, J., Li, Y., 2015. Talanta 132, 150–154.
Luo, Suxing, Wu, Yuanhui, Gou, Hua, 2013. Ionics 19 (4), 673–680.
Ma, R., Zhou, Y., Chen, Y., Li, P., Liu, Q., Wang, J., 2016. Angew. Chem. Int. Ed. 127 (49), 14936–14940.
Meszlényi, G., Körtvélyessy, J., Juhász, É., Lelkes, M., 1990. Analyst 115 (11), 1491–1493.
Nemeth-Konda, L., Füleky, G., Morovjan, G., Csokan, P., 2002. Chemosphere 48 (5), 545–552.
Oliveira, A.M., Loureiro, H.C., Jesus, F.F., de Jesus, D.P., 2017. J. Sep. Sci. 40 (7), 1532–1539.
Özlem, E., Selma, Ö., Ziya, Ö.Z., 2016. Sensors 16 (8), 1274.
Park, H., Encinas, A., Scheifers, J.P., Zhang, Y., Fokwa, B.P.T., 2017. Angew. Chem. Int. Ed. 56 (20), 5575–5578.
Poorahong, S., Izquierdo, R., Siaj, M., 2017. J. Mater. Chem. 5 (39), 20993–21001.
Qi-Long, Z., Qiang, X., 2014. Chem. Soc. Rev. 43 (16), 5468–5512.
Roy, A., Martinez, U., Brosha, E.L., Atanassov, P., Ward, T.L., 2013. J. Electrochem. Soc. 15 1618-1618.
Samsudin, E.M., Hamid, S.B.A., Juan, J.C., Wan, J.B., Centi, G., 2016. Appl. Surf. Sci. 370, 380–393.
Sharma, S., Singh, N., Tomar, V., Chandra, R., 2018. Biosens. Bioelectron. 107, 76–93.
Singh, S.B., Foster, G.D., Khan, S.U., 2007. J. Chromatogr. A 1148 (2), 152–157.
Strickland, A.D., Batt, C.A., 2009. Anal. Chem. 81 (8), 2895.
Veneziano, A., Vacca, G., Arana, S., De, S.F., Rastrelli, L., 2004. Food Chem. 87 (3), 383–386.
Wang, C., Sun, L., Zhang, F., Wang, X., Sun, Q., Cheng, Y., Wang, L., 2017. Small 13 (32), 1701246.
Wei, C., Cheng, N., Liu, Q., Ge, C., Asiri, A.M., Sun, X., 2014. ACS Catal. 4 (8), 2658–2661.
Wu, C., Cheng, Q., Wu, K., 2015. Anal. Chem. 87 (6), 3294–3299.
Xu-Gang, W.U., Yuan, X., Pang, H.Y., 2008. Food Sci. (N. Y.) 5, 082.
Yang, R., Zhu, D., Wen, H., Fu, A., Zhao, Z., Dai, G., Miao, Z., Hu, Y., 2017. J. Sep. Sci. 40 (5), 1150–1157.
Yao, Y., Wen, Y., Zhang, L., Wang, Z., Zhang, H., Xu, J., 2014. Anal. Chim. Acta 831 (23), 38–49.
Yu, Y., Jiang, C., Mo, L., Tao, L., Xie, L., Jie, H., Li, T., Ning, D., Yan, F., 2016. Food Anal. Methods 10 (5), 1479–1487.
Yujing, G., Shaojun, G., Jing, L., Erkang, W., Shaojun, D., 2011. Talanta 84 (1), 60–64.
Zahid, O.K., Wang, F., Ruzicka, J.A., Taylor, E.W., Hall, A.R., 2016. Nano Lett. 16 (3), 2033–2039.
Zhai, Q., Zhang, X., Li, J., Wang, E., 2016. Nanoscale 8 (33), 15303–15308.
Zhang, L., Liu, Y., Song, H., Huang, B., Ye, B.C., Li, Y., 2016. Analyst 141 (15), 4625–4631.
Zhang, J., Liu, J., Zhang, Y., Yu, F., Wang, F., Peng, Z., Li, Y., 2018a. Microchim. Acta 185 (1), 78.
Zhang, R., Yang, Z., Deng, X., Sun, S., Li, Y., 2018b. Electrochim. Acta 271, 417–424 Electrochimica Acta 271.
Zhi, W.S., Fredrickson, K.D., Anasori, B., Kibsgaard, J., Strickler, A.L., Lukatskaya, M.R., Gogotsi, Y., Jaramillo, T.F., Vojvodic, A., 2016. Acs Energy Let 1 (3), 589–594.
Zourob, M.M., Eissa, S.H.H., 2017. Anal. Chem. 89 (5), 3138–3145.